

FLUTTER PREDICTION IN THE TRANSONIC FLIGHT REGIME WITH THE γ - Re_θ TRANSITION MODEL

Michael Fehrs*, Anna C.L.M. van Rooij* and Jens Nitzsche*

* Institute of Aeroelasticity
German Aerospace Center (DLR)
Bunsenstr. 10, 37073 Göttingen, Germany
e-mail: michael.fehrs@dlr.de, anouk.vanrooij@dlr.de, jens.nitzsche@dlr.de
web page: <http://www.dlr.de/ae/>

Key words: boundary layer transition, γ - Re_θ transition model, transonic flow, airfoil flutter, aerodynamic resonance.

Abstract. This paper presents a flutter analysis for the supercritical CAST 10-2 airfoil and the laminar NACA 64-008 airfoil in a flow with free boundary layer transition based on CFD computations. For transition prediction the γ - Re_θ transition model is used. The results are compared to fully turbulent results obtained with the SST k - ω model. Unsteady RANS computations at $Re_c = 2 \cdot 10^6$ are used to determine the aerodynamic derivatives, required to identify the flutter boundary for a 2 degree-of-freedom model. At the limits of the laminar drag bucket a decrease in flutter stability can be found for both airfoils and the given structural model. However, the limits of the laminar bucket are strongly influenced by the prescribed turbulence boundary conditions. In addition, an aerodynamic resonance and the possibility of a 1 degree-of-freedom flutter is found for the CAST 10-2 airfoil.

1 INTRODUCTION

The influence of the laminar-turbulent boundary layer transition on the dynamic aeroelastic stability (flutter) of laminar or supercritical airfoils has not been investigated intensively. This is especially the case for transonic flows. In the transonic flight regime standard aeroelastic tools like doublet lattice methods can not be used as they do not account for relevant non-linear flow effects (e.g. shock movement) [17]. One way to approach this problem is to use unsteady CFD computations: CFD results are used to generate an aerodynamic data basis for the flutter analysis. This data basis contains lift and moment coefficients for forced heave and pitch motion of the airfoil. The aerodynamic coefficients are transferred to the frequency domain and used in a frequency matching method [17] to compute the flutter boundary of the airfoil.

This paper investigates the flutter behavior of a supercritical airfoil (CAST 10-2) and a laminar airfoil (NACA 64-008) at transonic Mach numbers. Unsteady fully turbulent and transitional CFD computations for a two degree-of-freedom (dof) airfoil model at a chord Reynolds number of $Re_c = 2 \cdot 10^6$ are used to generate the required aerodynamic data basis for the flutter analysis. For transition prediction the γ - Re_θ transition model in combination with the SST k - ω model is used in the DLR TAU code. The TAU code is a finite-volume solver for viscous and inviscid flows, which uses an edge-based dual-cell approach. It offers different eddy viscosity turbulence models to solve the Reynolds averaged Navier-Stokes (RANS) equations [14].

In wind tunnel tests at the DLR long transitional boundary layer regions were detected at transonic Mach numbers for the CAST 10-2. In addition, an aerodynamic resonance and the possibility for a one degree-of-freedom flutter was found [8]. First investigations with the γ - Re_θ transition model are able to reproduce the aerodynamic resonance qualitatively [6]. The resonance resembles these found in transonic separated flows [13], although there is no separation or shock in the given case on the airfoil surface [6].

For high Reynolds numbers one has to rely on RANS models for turbulence modeling and transition models for the transition prediction. In the γ - Re_θ transition model the transition onset is correlated to the turbulence intensity Tu and the pressure gradient outside the boundary layer [11]. The transition model adds two transport equations to the underlying turbulence model (e.g. SST k - ω model): The first provides the information about the critical flow quantity for the transition onset ($\tilde{Re}_{\theta t}$ -transport equation). The second enables the comparison between local boundary layer quantities and the transition criterion to detect the transition onset (γ -transport equation). The intermittency variable γ is used to increase the turbulence kinetic energy in the boundary layer. A complete description of the transition model can be found in [10]. The model is implemented into the TAU code and results and comparisons to the e^N -method can be found in [15].

Up to a free stream Mach number of $Ma = 2$ compressibility has a stabilizing effect on 2d, natural transition [1]. The transition model does not account specifically for compressibility effects as no appropriate transonic/supersonic/hypersonic test case is used for calibrating the transition correlations. Nevertheless, [9] found that by calibrating the model with subsonic flat plate test cases the obtained correlations are working well for hypersonic double ramp test cases. In [7] the γ - Re_θ transition model is used without any compressibility correction to predict the free boundary layer transition in subsonic and transonic flow over the NLR-7301. It is concluded that the predicted transition positions agree satisfactory with experimental results up to $Ma = 0.7$. For higher transonic Mach numbers it is assumed that the accuracy of the turbulence model to capture shock-induced separation gives rise to the differences in the predicted transition position. For these higher Mach numbers the presented pressure distributions do not match the experimental data.

It will be shown that a decrease in flutter stability is found using the γ - Re_θ transition model in the transonic flight regime when the limit of the laminar bucket is reached.

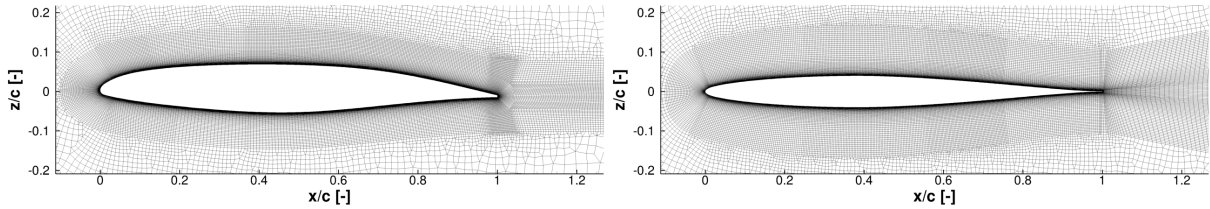


Figure 1: Computational grid in the vicinity of the airfoil for the CAST 10-2 (left) and NACA 64-008 (right).

2 INVESTIGATION SET-UP

2.1 Aerodynamic model and numerical method

The design point for the CAST 10-2 is $Ma = 0.76$ at $\alpha = 0.3^\circ$ and $c_l = 0.595$ [16]. The airfoil coordinates are given in [5]. The section coordinates for the NACA 64-008 are taken from [2]. The airfoil has a sharp trailing edge. However, in the course of the investigation it was found that a blunt trailing edge strongly improves the grid quality and numerical convergence. Therefore the NACA airfoil was altered to have a blunt trailing edge with a thickness of $t/c = 0.001$.

The flow around both airfoils is investigated at a chord Reynolds number of $Re_c = 2 \cdot 10^6$. For the CFD computations a 2d grid is used with a structured grid in the vicinity of the airfoil and an unstructured grid for the remaining flow field. The grid plane for the CAST 10-2 contains roughly 60 000 grid points. The height of the first cell gives a maximum y^+ value of about 1.3. Lowering the y^+ value showed no significant effect on the aerodynamic coefficients. The grid plane for the NACA 64-008 contains about 70 000 grid points with a similar distribution in stream wise direction as for the CAST 10-2. The height of the first cell gives a maximum y^+ value of about 0.3. In both cases the far field boundary is 100 chord lengths away from the airfoil. The cell length Δx_l in stream wise direction over chord length c is $\Delta x_l/c = 0.004$ on the upper surface for both airfoils. The grid on the lower surface of the CAST 10-2 is slightly coarser. Figure 1 depicts both grids in the vicinity of the airfoils.

For the fully turbulent flow the SST $k-\omega$ turbulence model is used. This allows a better comparison to the free transition computations as the $\gamma-Re_\theta$ model is used for transition prediction with the SST $k-\omega$ model as the underlying turbulence model. A central, second order scheme with scalar dissipation is used for the discretization of the convective fluxes of the RANS equations. For the convective fluxes of the turbulence equations a first order Roe upwind scheme is used. The turbulence boundary conditions for the $\gamma-Re_\theta$ transition model are chosen to obtain a turbulence intensity in the vicinity of the airfoil of about $Tu \approx 0.1\%$.

The pitch and heave motions are given by a simple sine for different reduced frequencies $k = \omega \cdot c/U$. For the pitch motion an amplitude of $\alpha_a = 0.05^\circ$ is prescribed. The amplitude of the heave motion h_a is chosen to give an effective angle of attack $\alpha_{\text{eff}} = k \cdot h_a/c$ of the

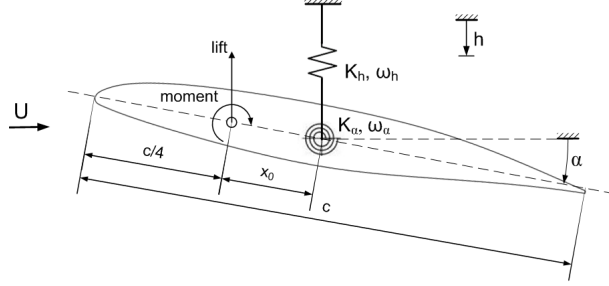


Figure 2: Two dof airfoil model for the flutter analysis.

same magnitude as α_a for every reduced frequency. For all reduced frequencies 5 periods are computed. Lift and moment of the last period are transferred to the frequency domain by a fourier transform. The complex valued 1st harmonic is used as input for the flutter analysis. The time step number per period varies with reduced frequency to give the same time step size for every computation.

2.2 Flutter analysis and structural model

The flutter analysis is based on the 2 dof system shown in figure 2. The airfoil moves in heave and pitch motion around its quarter chord ($x_0 = 0$). The described model will encounter classical bending-torsion flutter for certain flow and structural parameters [3]. The equation of motion for the given system can be written in a non-dimensional form:

$$\left([\mathbf{M}^*] - \lambda \left\{ 1 + 2i \begin{bmatrix} \delta_h & 0 \\ 0 & \delta_\alpha \end{bmatrix} \right\} [\mathbf{K}^*] + \frac{2}{\mu\pi k^2} [\mathbf{A}^*] \right) \begin{bmatrix} \hat{h} \\ \hat{\alpha} \end{bmatrix} = 0, \quad (1)$$

with the non-dimensional mass $[\mathbf{M}^*]$, stiffness $[\mathbf{K}^*]$, and aerodynamic matrices $[\mathbf{A}^*]$:

$$[\mathbf{M}^*] = \begin{bmatrix} 1 & x_\alpha \\ x_\alpha & r_\alpha^2 \end{bmatrix}, \quad [\mathbf{K}^*] = \begin{bmatrix} \omega_h^2/\omega_\alpha^2 & 0 \\ 0 & r_\alpha^2 \end{bmatrix}, \quad [\mathbf{A}^*] = \begin{bmatrix} -c_{lh}c & -c_{l\alpha} \\ c_{mh}c & c_{m\alpha} \end{bmatrix}, \quad (2)$$

The structural parameters are chosen in accordance with [4], except a change is made to the mass moment of inertia about the elastic axis. The mass moment of inertia is doubled to obtain flutter for all cases.

Equation 1 constitutes an eigenvalue problem for the reduced frequency parameter $\lambda = \omega_\alpha^2/\omega^2$. The frequency and damping of each mode are given by the real and imaginary part of the corresponding eigenvalue λ :

$$\Omega = \frac{\omega_\alpha}{\Re\{\sqrt{\lambda}\}}, \quad (3)$$

$$\delta = \frac{\Im\{\sqrt{\lambda}\}}{\Re\{\sqrt{\lambda}\}}. \quad (4)$$

In the k-method the reduced frequency k in eq. 1 is varied until it matches the resulting reduced frequency for Ω from eq. 3. The complex-valued aerodynamic derivatives in eq. 1

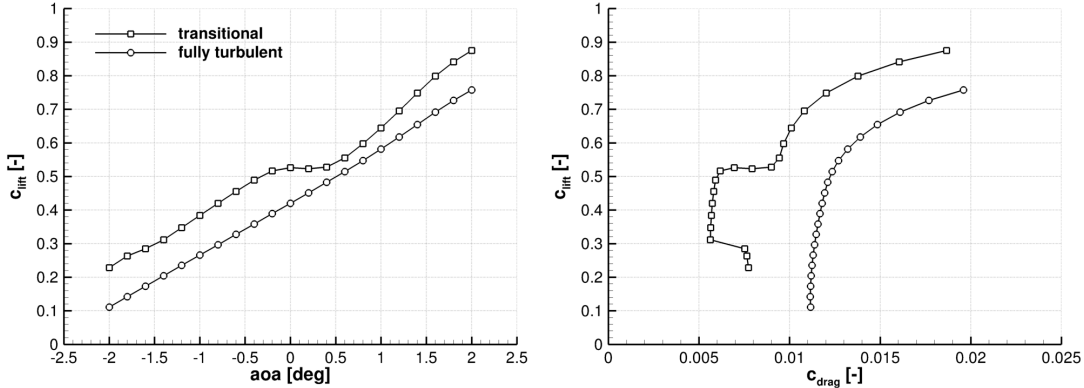


Figure 3: Lift and drag curve for the CAST 10-2 at $Ma = 0.72$.

(c_{lh} , $c_{l\alpha}$, c_{mh} , $c_{m\alpha}$) are unknown and depend on the reduced frequency. They are obtained by forced motion CFD computations. The aerodynamic matrix $[\mathbf{A}^*(k)]$ is found by an interpolation between the computed coefficients for different reduced frequencies.

To obtain the airfoil's flutter boundary the mass ratio μ_m is varied for a given Mach number, Reynolds number and structural model. The damping found for each flight condition has to be interpreted as a structural damping to give zero overall damping [17]. This means that a positive value describes an unstable flight condition. The conditions where the damping gets positive for a non-zero frequency are usually expressed by the flutter index Fi :

$$Fi = \frac{2U}{\sqrt{\mu_m} c \omega_\alpha}. \quad (5)$$

3 RESULTS

3.1 Steady results

In this section the steady CFD results for the CAST 10-2 and NACA 64-008 airfoil are presented. Figures 3 and 4 show the lift and drag curve for the CAST 10-2 and the NACA 64-008 airfoil at transonic Mach numbers respectively. The CAST 10-2 shows a high lift and drag benefit from the laminar flow. However, when the upper limit of the laminar bucket is reached ($\alpha \approx -0.2^\circ \dots 0.6^\circ$) the lift coefficient decreases as the transition location changes to an upstream position on the upper side of the airfoil.

The effect of the laminar bucket limit on the lift and drag coefficients for the NACA 64-008 is less significant. The different transition positions on the upper and lower side of the airfoil for a non-zero angle of attack give an effective rear camber of the airfoil. At an angle of attack of $\alpha = 2^\circ$ the transition position changes on the upper side of the airfoil. For an increasing angle of attack the transition position moves upstream. The thickening boundary layer changes the effective rear camber and the lift curve shifts. At the same time, the drag coefficient rises. Nevertheless, the drag benefit compared to a

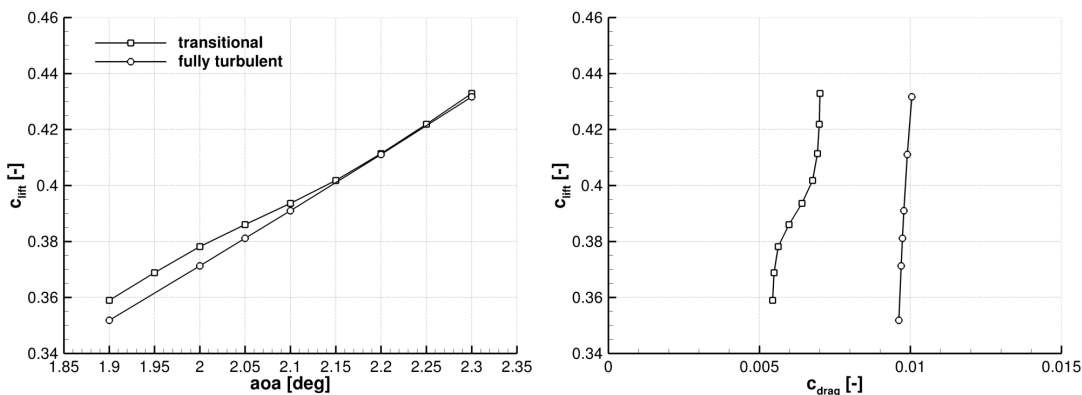


Figure 4: Lift and drag curve for the NACA 64-008 at $\text{Ma} = 0.75$.

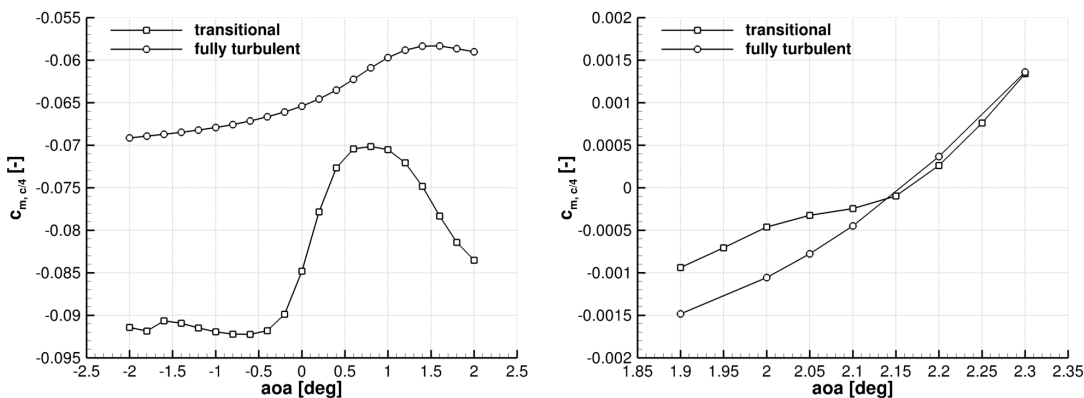


Figure 5: Transitional and fully turbulent moment coefficient for the CAST 10-2 (left) and the NACA 64-008 (right).

fully turbulent boundary layer is still high as the laminar boundary extends to $x/c \approx 0.75$ on the lower surface of the airfoil.

Figure 5 depicts the transitional and fully turbulent moment coefficient for the CAST 10-2 and the NACA 64-008. For the transonic flow over the CAST 10-2 the variation over the laminar bucket is more significant than for the NACA airfoil. For angles of attack above the laminar bucket limit there is still a strong non-linear behavior of the lift and moment coefficient for the CAST 10-2.

The pressure and skin friction coefficients for the CAST 10-2 at $\text{Ma} = 0.72$, $\alpha = 0^\circ$ and the NACA 64-008 at $\text{Ma} = 0.75$, $\alpha = 2^\circ$ are given in figure 6. In both cases the transition model increases the intermittency γ at an early position ($c_{f,\min}$). The boundary layer shows a long transitional region on the upper surface of the airfoil. This is caused by the vanishing (CAST 10-2) or slightly adverse (NACA 64-008) pressure gradient. In case of the CAST 10-2 the flow over the airfoil's upper surface is transonic and shock free in the turbulent and transitional case. The turbulent flow over the NACA 64-008 at $\alpha = 2^\circ$

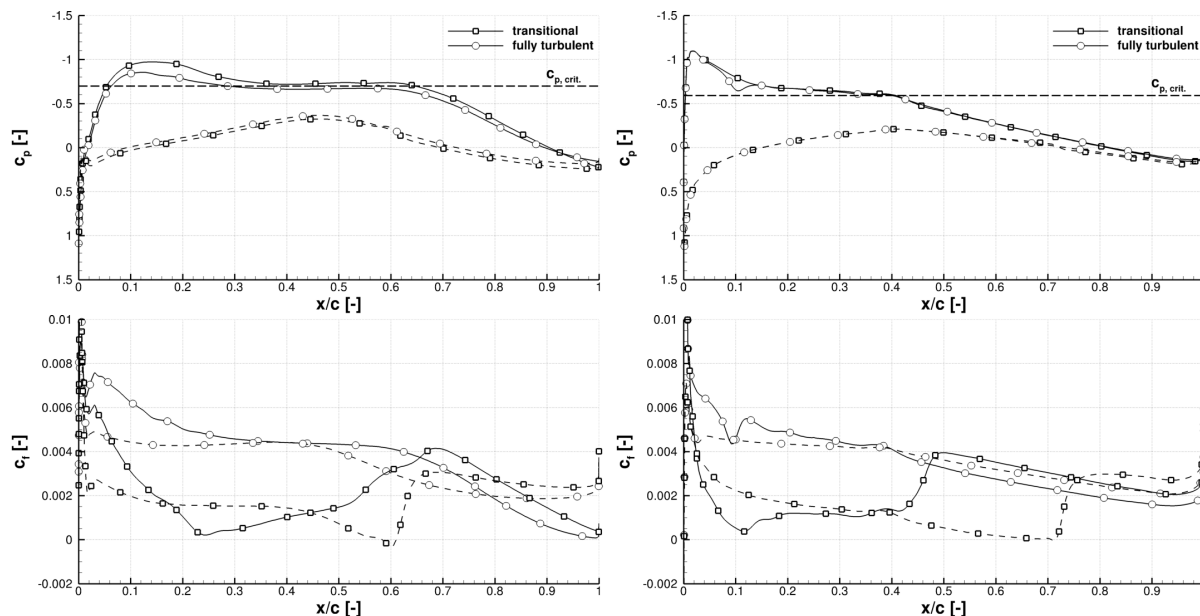


Figure 6: Pressure and friction coefficient distribution for the CAST 10-2 at $Ma = 0.72$, $\alpha = 0^\circ$ (left) and the NACA 64-008 at $Ma = 0.75$, $\alpha = 2^\circ$ (right). The lower surface is given by the dashed line.

shows a weak shock at $x/c \approx 0.1$, but stays sonic to almost 40 % chord length. The transitional flow is shock free and shows the same extend of sonic flow above the airfoil as the fully turbulent flow.

3.2 Turbulence level and laminar bucket

For transition prediction with the γ - Re_θ transition model a sound choice for the turbulence boundary conditions must be made. The turbulence can be described by the turbulence intensity Tu and the viscosity ratio $R_T = \mu_t/\mu$. The turbulence boundary conditions have to be chosen so that in the vicinity of the airfoil the desired turbulence level is reached. The turbulence decay is determined in a constant velocity flow by the destruction terms of the turbulence equations. For a stationary flow with constant density the decay of turbulence intensity is given by:

$$Tu_0 = Tu_{in} \left(1 + \frac{3\rho U \Delta x \beta_2 Tu_{in}^2}{2\mu (\mu_t/\mu)_{in}} \right)^{-\beta^*/(2\beta_2)}, \quad (6)$$

with constants β_2 and β^* from the SST k - ω turbulence model [12]. Eq. 6 gives the theoretical turbulence intensity Tu_0 for a given Δx if the turbulence intensity Tu_{in} and the viscosity ratio $R_{T,in}$ are specified at the inflow boundary. Although equation 6 is exact for a free flow field, it can not predict the turbulence levels in the direct vicinity of an airfoil.

Fig. 7 shows the actual turbulence intensity Tu at $Ma = 0.72$ at $\alpha = 0^\circ$ for the CAST 10-2 in the vicinity of the airfoil. For the case on the left the boundary conditions are

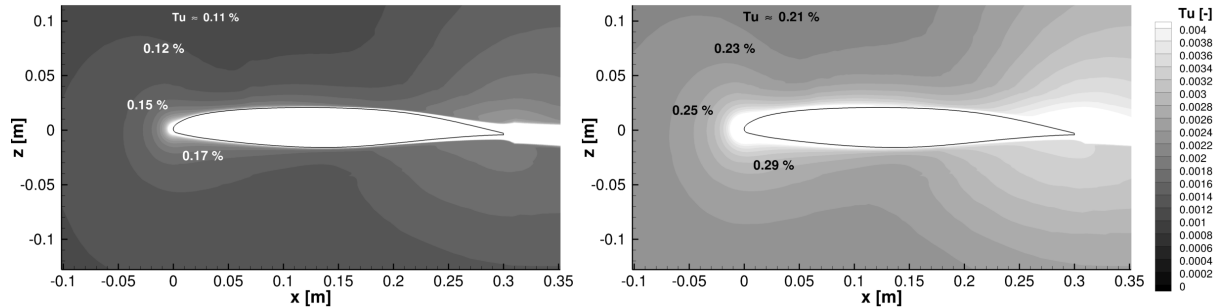


Figure 7: Actual turbulence intensity in the vicinity of an airfoil: On the left the inflow boundary conditions Tu_{in} and $R_{T,in}$ are set to obtain a theoretical turbulence intensity of $Tu_0 = 0.1\%$. On the right the boundary conditions are set to obtain a value of $Tu_0 = 0.2\%$.

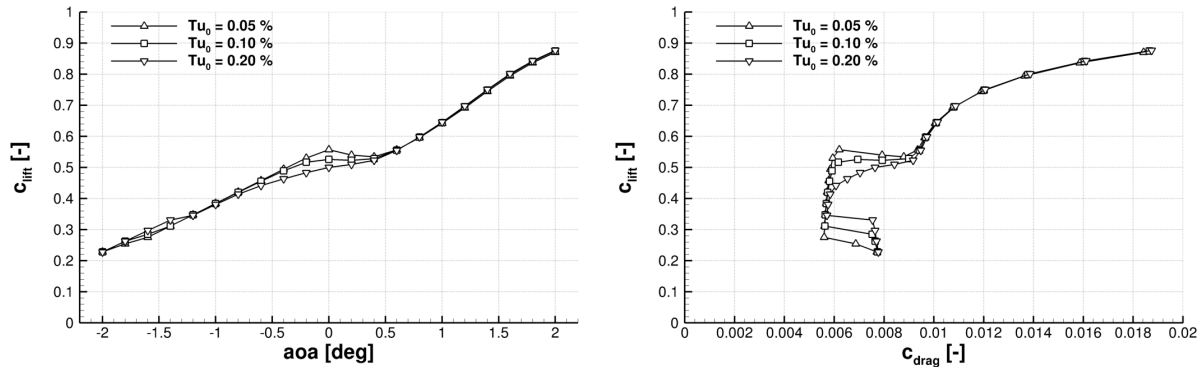


Figure 8: Influence of different theoretical turbulence intensities Tu_0 on the laminar bucket.

chosen to obtain a theoretical turbulence intensity of $Tu_0 = 0.1\%$ and in the case on the right of $Tu_0 = 0.2\%$. Above the airfoil the desired condition is obtained. However, in the vicinity of the airfoil the turbulence intensity increases far above the desired value. For a given flow the theoretical turbulence intensity Tu_0 can deviate strongly from the actual turbulence intensity near the airfoil. In addition, the viscosity ratio must be unphysical high on the boundaries to obtain a certain turbulence level at the airfoil's position.

Fig. 8 shows the influence of the freestream turbulence level on the laminar bucket for the CAST 10-2 at $Ma = 0.72$. The boundary conditions are set to obtain a theoretical turbulence intensity by equation 6 of $Tu_0 = 0.05\%$, 0.1% , and 0.2% . An increase in turbulence gives a narrower laminar bucket, although the minimum drag inside the bucket is not affected. For $Tu_0 = 0.05\%$ the transition position on the upper side of the airfoil shows a rapid change at the upper limit of the laminar bucket, whereas there is a smooth transition movement for $Tu_0 = 0.2\%$.

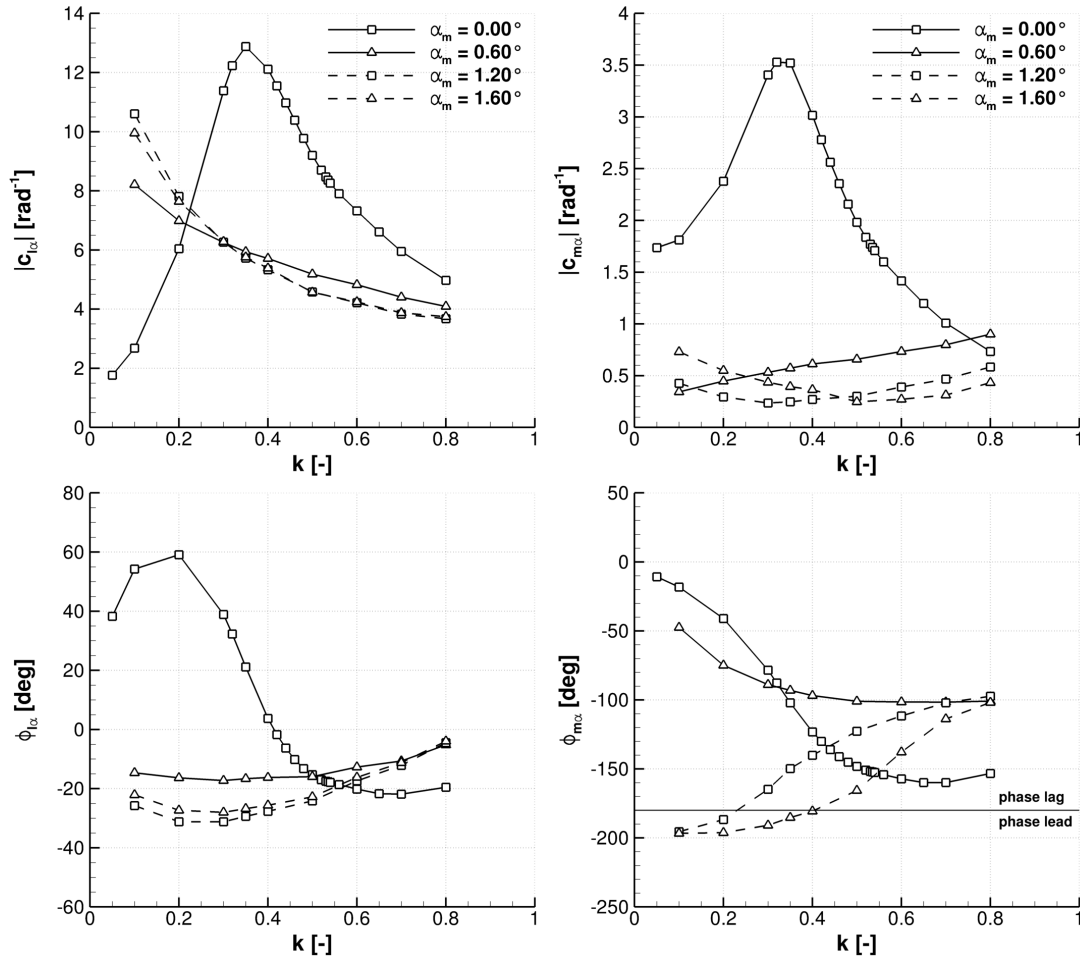


Figure 9: CAST 10-2 airfoil, $Ma = 0.72$ at different mean angles of attack: Magnitude and phase for the lift (left) and moment (right) coefficient derivative due to pitch motion for the transitional flow.

3.3 Unsteady results and flutter analysis

For both airfoils the flutter stability is investigated for different mean angles of attack at the upper limit of the laminar bucket. The transitional results are compared to fully turbulent results. The fully turbulent computations are limited to fewer mean angles of attack as the variation in the lift and moment curve slope in the considered angle of attack range is weak.

In case of the CAST 10-2 significant changes can be found in the amplitude and phase response as the laminar drag bucket is left. Figure 9 depicts the magnitude and phase of the moment coefficient due to pitch for a transitional flow at different mean angles of attack. For $\alpha_m = 0^\circ$ one finds a pronounced aerodynamic resonance maximum at $k = 0.35$. During one pitch or heave period the length of the transition region changes strongly on the upper side of the airfoil for this mean angle of attack and reduced frequency. The

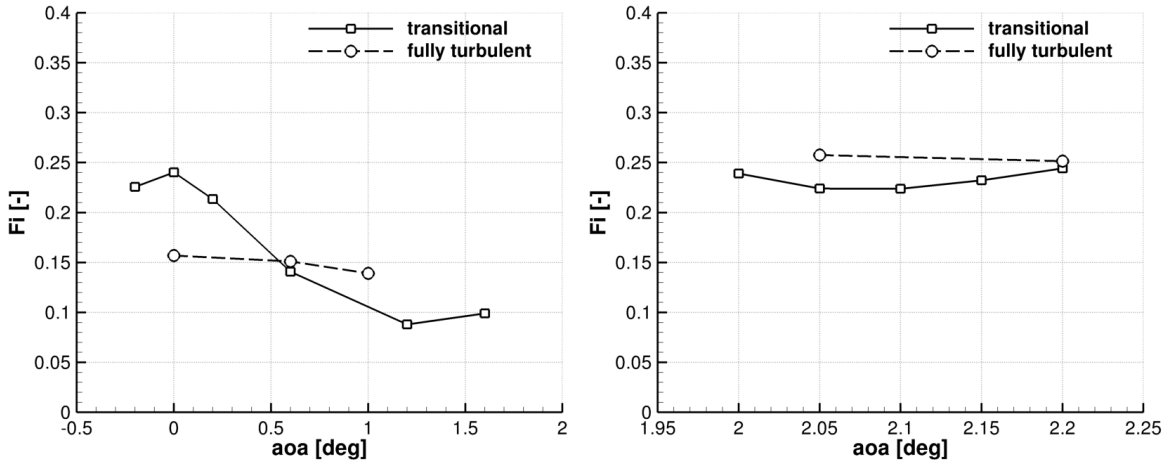


Figure 10: Flutter index for both airfoils in the upper limit of the laminar bucket. Left: CAST 10-2 at $Ma = 0.72$. Right: NACA 64-008 at $Ma = 0.75$.

flow is shock and separation free on the upper side of the airfoil for the whole pitch and heave period.

For $\alpha_m = 0.6^\circ$ the transitional results resemble the fully turbulent data (not depicted). As the mean angle of attack is increased (and the upper limit of the bucket is left) the moment coefficient response changes and one finds a phase lead (positive imaginary part of $c_{m\alpha}$) for low reduced frequencies. The phase lead range increases as the mean angle of attack is further increased. A phase lead of the moment coefficient makes a 1 dof torsion flutter possible [3]. In [8] the phase lead is also found as the upper limit of the laminar bucket is left. The flow over the NACA 64-008 shows no such effect.

The flutter boundary for both airfoils is presented in figure 10. On the left hand side the results for the CAST 10-2 at $Ma = 0.72$ are presented and on the right hand side the results for the NACA 64-008 at $Ma = 0.75$. As the upper limit of the laminar bucket is reached the flutter stability lowers in both cases for the given structural model. The loss in flutter stability is more dramatic in case of the CAST 10-2. At a mean angle of attack of $\alpha_m = 0^\circ$ and 0.2° the torsional (second) mode becomes unstable. In case of the NACA 64-008 the heave mode determines the flutter boundary for all cases. For $\alpha_m = 2.2^\circ$ the transitional flutter index reaches values similar to the fully turbulent result as can be expected from the steady and unsteady data.

4 CONCLUSIONS

This paper presents a flutter analysis for the supercritical CAST 10-2 and the laminar NACA 64-008 airfoil with free boundary layer transition based on CFD computations with the γ - Re_θ transition model. The results are compared to results obtained by fully turbulent simulations with the SST k - ω model. Unsteady RANS computations at $Re_c = 2 \cdot 10^6$ are used to determine the aerodynamic derivatives, required to solve the flutter

equation for a 2 dof model by a k-method. It is found that the flutter boundary decreases for a flow with free boundary layer transition when the limit of the laminar bucket is reached.

The CAST 10-2 results show that the turbulence level has a strong impact on the transition behavior. Small changes in the turbulence level can change the extend of the laminar bucket and the aerodynamic coefficient derivatives at the limits of the bucket. For a given wind tunnel the identification of an appropriate turbulence level in the vicinity of an airfoil is problematic as the turbulence level is changed by the airfoil itself. The influence of the turbulence level on the derivatives of the aerodynamic coefficients adds uncertainties in the aeroelastic predictions. For aeroelastic consideration not only the occurrence of the transonic dip [17] has to be taken into account but also the dip that might be given by the laminar drag bucket limit.

The γ - Re_θ transition model is able to reproduce the effects in the transonic flight regime for the supercritical CAST 10-2 found in wind tunnel data [8]: one finds long transitional regions, an aerodynamic resonance, and the possibility of a 1 dof torsion flutter.

The flutter boundary of the CAST 10-2 will be investigated in the transonic wind tunnel Göttingen (DNW-TWG). The aerodynamic CFD data basis will be used in flutter computations with the structural model of the CAST 10-2 wind tunnel model. This will give the opportunity to validate the predicted flutter behavior trends at the laminar drag bucket limit.

REFERENCES

- [1] Arnal, D. and Vermeersch, O. Compressibility effects on laminar-turbulent boundary layer transition. *45th Symposium of Applied Aerodynamics* (2010), 22nd – 24th March, Marseille, France.
- [2] Abbott, I., von Doenhoff, A.E. and Stivers L.S. (Jr.) Summary of Airfoil Data. NACA (1945) Report 824.
- [3] Bisplinghoff, R.L., Ashley, H. and Halfman, R.L. *Aeroelasticity*. Dover Publications, New York (USA), Vol. I., (1996).
- [4] Dietz, G., Schewe, G. and Mai, H. Experiments on heave/pitch limit-cycle oscillations of a supercritical airfoil close to the transonic dip. *Journal of Fluid and Structures* (2004) **19**(1): 1–16.
- [5] Dress, D.A., Johnson, C.B., McGuire, P.D., Stanewsky, E. and Ray, E.J. High Reynolds Number Tests of the CAST 10-2/DOA 2 Airfoil in the Langley 0.3-Meter Transonic Cryogenic Tunnel - Phase I. *NASA Langley Research Center* (1983), Technical Memorandum TM-84620, Hampton, Virginia (USA).
- [6] Fehrs, M. Influence of Transitional Flows at Transonic Mach Numbers on the Flutter Speed of a Laminar Airfoil. In: *Proc. IFASD* (2013), 21B.

- [7] Gang Wang, Haris Hameed Mian, Zheng-Yin Ye and Jen-Der Lee. Numerical Study of Transitional Flow Around NLR-7301 Airfoil Using Correlation-Based Transition Model. *Journal of Aircraft* (2014) **51**(1): 342–349.
- [8] Hebler, A., Schojda, L., and Mai, H. Experimental Investigation of the Aeroelastic Behavior of a Laminar Airfoil in Transonic Flow. In: *Proc. IFASD* (2013), 32C.
- [9] Krause, M., Behr, M. and Ballmann, J. Modeling of Transition Effects in Hypersonic Intake Flows Using a Correlation-Based Intermittency Model. *15th AIAA International Space Planes and Hypersonic Systems and Technologies Conference* (2008), AIAA 2008-2598, 28th April – 1st May, Dayton, Ohio (USA).
- [10] Langtry, R.B. A Correlation-based Transition Model Using Local Variables for Unstructured Parallelized CFD Codes. *University Stuttgart* (2006), Ph.D. thesis.
- [11] Langtry, R.B. and Manter, F.R. Correlation-based Transition Modeling for Unstructured Parallelized Computational Fluid Dynamics Codes. *AIAA Journal* (2009) **47**(12): 2894 – 2906.
- [12] Menter, F.R. Two-Equation Eddy-Viscosity Turbulence Models for Engineering Applications. *AIAA Journal* (1994) **32**(8): 1598–1605.
- [13] Nitzsche, J. A Numerical Study of Aerodynamic Resonance in Transonic Separated Flow. In: *Proc. IFASD* (2009), IFASD-2009-126.
- [14] Schwammborn, D., Gerhold, T. and Heinrich, R. The DLR Tau-code: Recent Applications in Research and Industry. In: *Proc. European Conference on Computational Fluid Dynamics ECCOMAS* (2006), Netherlands.
- [15] Seyfert, C., Krumbein, A. Evaluation of a Correlation-based Transition Model and Comparison with the e^N -method. In: *40th Fluid Dynamics Conference and Exhibit* (2010), AIAA 2010-4443, 28th June – 1st July, Chicago, Illinois (USA).
- [16] Stanewsky, E., Demurie, F., Ray, E.J. and Johnson, C.B. High Reynolds number tests of the CAST-10-2/DOA 2 transonic airfoil at ambient and cryogenic temperature conditions. *AGARD Conference Proceedings: Wind Tunnels and Testing Techniques* (1984) No. 348: 47–60.
- [17] Wright, J.R. and Cooper, J.E. *Introduction to Aircraft Aeroelasticity and Loads*. John Wiley & Sons, West Sussex (GB), Vol. I. (2007).